Supporting Information

Ultrathin conjugated Microporous Thermoset Nanosheets for Efficient Li-ion Storage

Yantuo Li,[†a] Yuzhe Sun, [†a] Jinshu Zhang, [a] Yang Yang,[a] Jianxue Wu,[a] Mingyi Ning,[a] and Wei Liu*[a, b]

[a]School of Physics, Key Laboratory of Quantum Materials and Devices of Ministry of Education, Frontiers Science Center for Mobile Information Communication and Security

Southeast University

Nanjing 211111, China

[b]Purple Mountain Laboratories

Nanjing 211111, China

*Corresponding email address: 101012931@seu.edu.cn

† These authors contributed equally to this work

Materials characterizations

The shape and morphology of CMT-n were examined using scanning electron microscopy (SEM) with an FEI Inspect F50. Elemental mappings were analyzed through energy dispersive spectrometry (EDS) connected to the SEM. The morphology and thickness of CMT-n were further investigated using atomic force microscopy (AFM) with a Bruker Dimension Icon Atomic Force Microscope. N2 adsorption and desorption isotherms were measured at 77.3 K using a Micromeritics ASAP 2020 HD88, and pore size distributions were calculated by the Barrett-Joyner-Halenda (BJH) method. X-ray diffraction (XRD) patterns were acquired on a Rigaku Smart-lab X-ray diffractometer using Cu Kα radiation (λ=1.5406 Å). Fourier-transform infrared spectroscopy (FTIR) was performed with a IRTracer-100 spectrometer. High-resolution transmission electron microscopy (HRTEM) images were obtained using the Talos F200X. Solid 13C NMR spectra were recorded with Bruker Avance II 600. X-ray photoelectron spectroscopy (XPS) data were collected with an ESCALAB 250 XI (Thermo Kalpha) equipped with mono Al Kα. Raman spectra were obtained using a Lab RAM HR UV-visible Raman Microprobe. Inductively coupled Plasma Mass Spectrometry (ICP-MS) with Agilent 7700s

Coin cells assembly and electrochemical performance measurements

Electrochemical measurements of half-cells were conducted using CR2032 coin cells at 25 °C. All cells were assembled in an argon-filled glove box, maintaining H2O and O2 levels below 0.01 ppm. Charge-discharge tests were performed using the LAND test system at various current densities within a voltage window of 0.01 to 2.50 V versus Li^+/Li at room temperature. Prior to cycle tests, the batteries were activated for three cycles at 0.5 A g^{-1}. Cyclic voltammetry (CV) measurements were carried out using an electrochemical workstation (Chenhua Instrument, CHI760E). Sodium tablets were employed as reference and counter electrodes, and glass fiber was used as the separator. The working electrodes were prepared by mixing CMT-n, Super P, and polyvinylidene fluoride (PVDF) in a mass ratio of 7: 2: 1 with N-methyl-pyrrolidone (NMP). The mixture was stirred for 12 hours to form a uniform slurry, which was then coated onto Cu foil and vacuum dried at 120 °C overnight. The mass loading of CMT-n on each anode was approximately 1 mg cm^{-2}. The electrolyte consisted of 1 M LiPF4 in a 1:1 (v/v) mixture of ethylene carbonate (EC) and dimethyl

carbonate (DMC), supplemented with 2% fluoroethylene carbonate (FEC).

Calculation of the Diffusion Coefficient

Use Fick's second law to calculate the diffusion coefficient (D) with the following formula: where:

$$D = \frac{4}{\pi}\left(\frac{n_m}{F}\right)^2\left(\frac{I}{A}\right)^2\left(\frac{\tau}{(\Delta E\tau/\Delta Es)^2}\right)$$

n_m is the number of lithium ions in the material.

F is the Faraday constant.

I is the applied constant current.

A is the area of the electrode.

τ is the duration of the current pulse.

$\Delta E\tau$ is the voltage change during the current pulse.

ΔEs is the steady-state open-circuit voltage change.

Supporting Figures

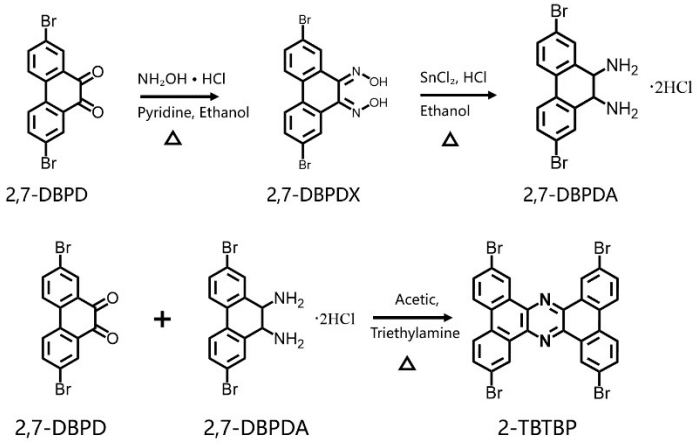

Figure S1. Molecular design of 2-TBTBP

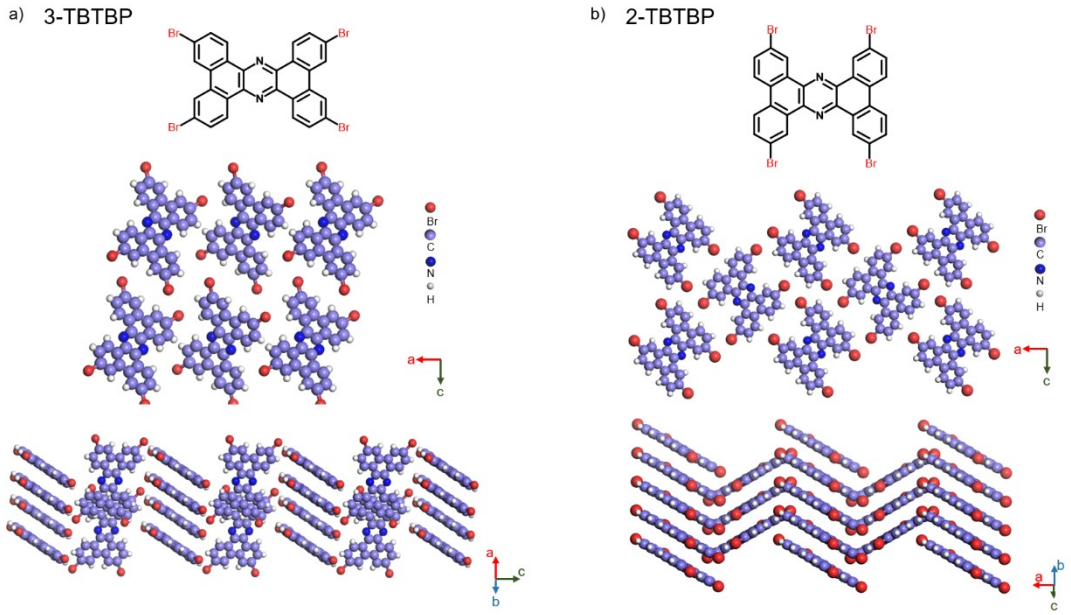

Figure S2. Crystal structures of 3-TBTBP (Melting peak at ~509 °C) [1]and 2-TBTBP (Melting peak at ~530 °C), a) Top view along b-axis and side view. [1]b) Top view along b-axis and side view.[2]

Even though 2-TBTBP and 3-TBTBP have identical molecular weight and chemical composition, the slight variation in the position of C-Br bonds results in different molecular packing. This difference leads to distinct binding energy in the two molecular crystals (-620.84 eV for 2-TBTBP vs -620.768 eV for 3-TBTBP). The binding energies were calculated using the following method: The binding energy is typically expressed as a negative value, indicating energy release. The formula for binding energy is:

$E_{binding} = E_{molecule} - \sum E_{atoms}$

Where $E_{binding}$is the binding energy, $E_{molecule}$is the total energy of the molecule, and $\sum E_{atoms}$ are the energy of all the atoms contained within the molecule.

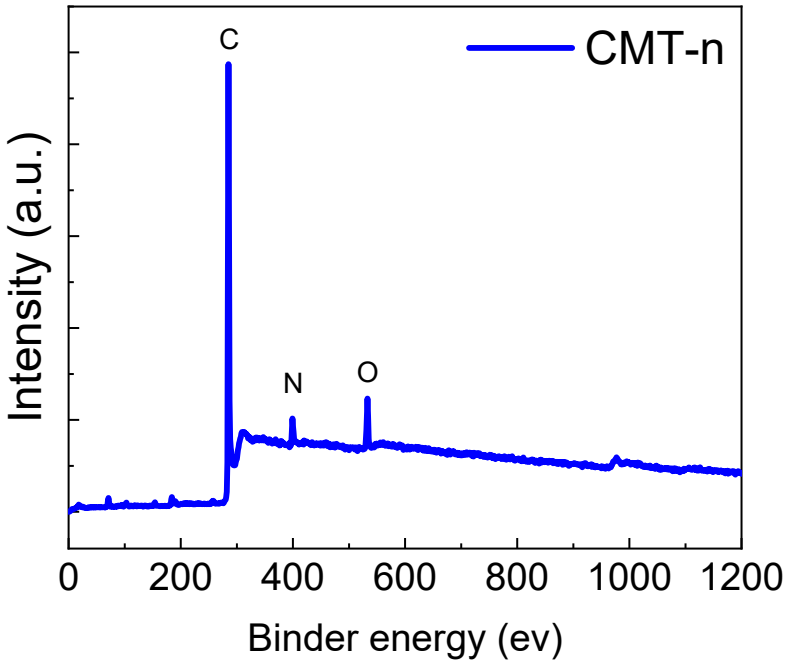

Figure S3. XPS spectrum of CMT-n.

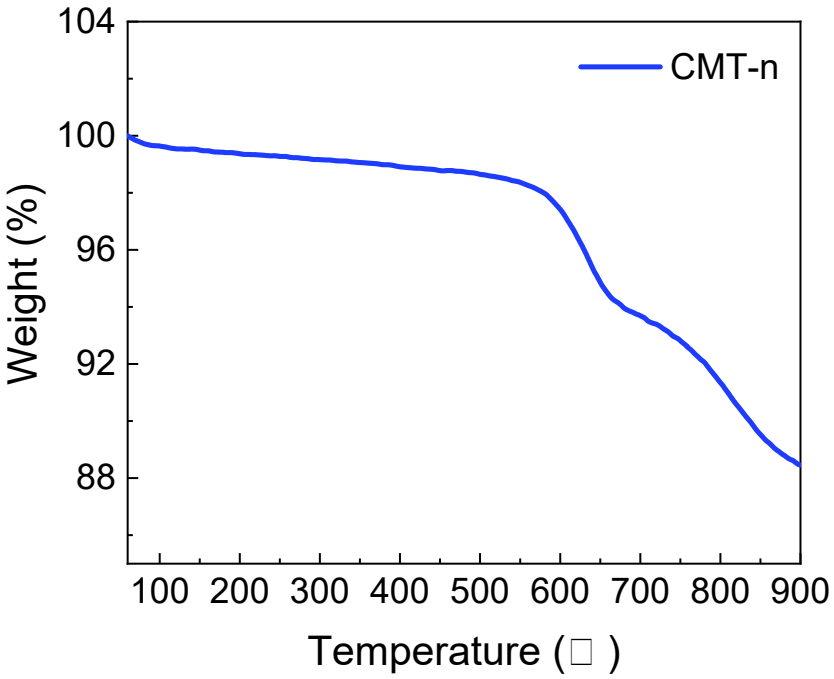

Figure S4. TG of CMT-n. Thermogravimetric analysis (TGA) of CMT-n, as shown in Supplementary Figure S4, indicates that the material remains thermally stable up to 600°C, with negligible weight loss observed in this temperature range. This high thermal stability is attributed to the robust polymeric framework of CMT-n.

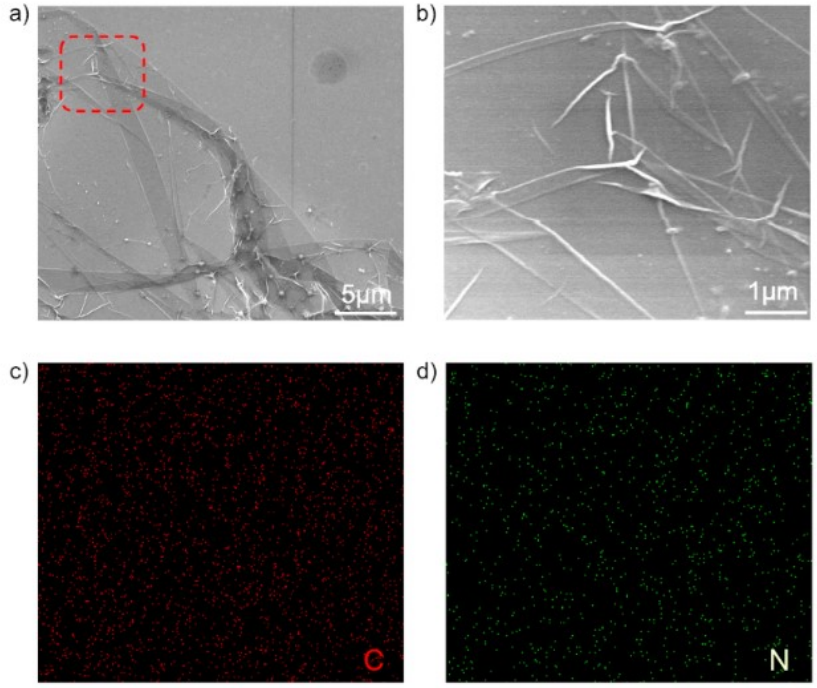

Figure S5. a) SEM image of CMT-n, and b) Enlarged SEM image of the red dashed square in (a). c, d) Elemental mapping of C and N in Figure S3b

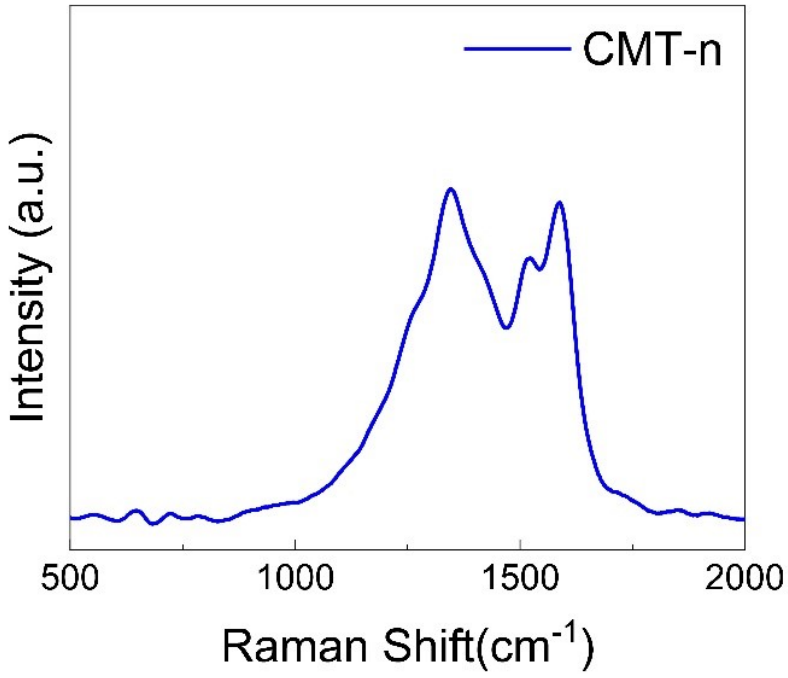

Figure S6. Raman spectrum of CMT-n.

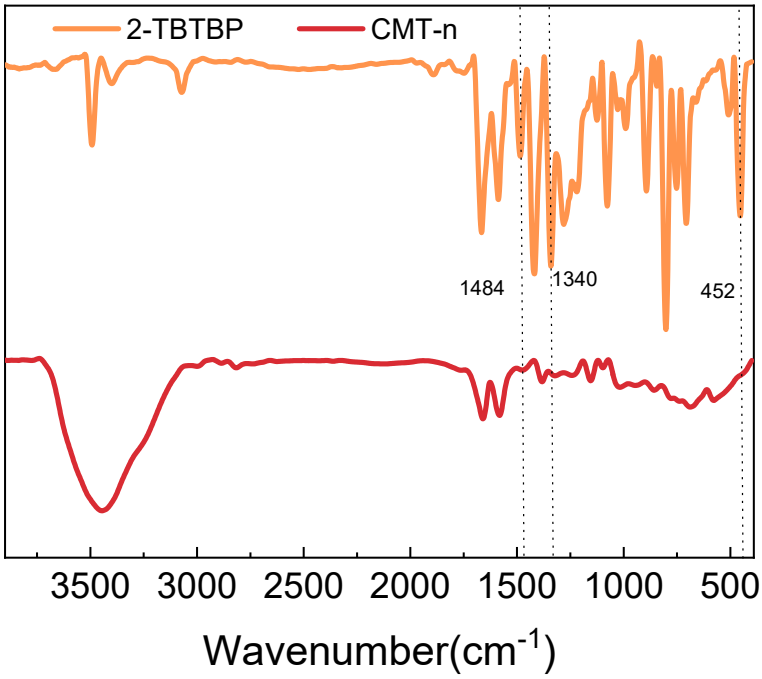

Figure S7. FTIR spectra of 2-TBTBP and CMT-n.

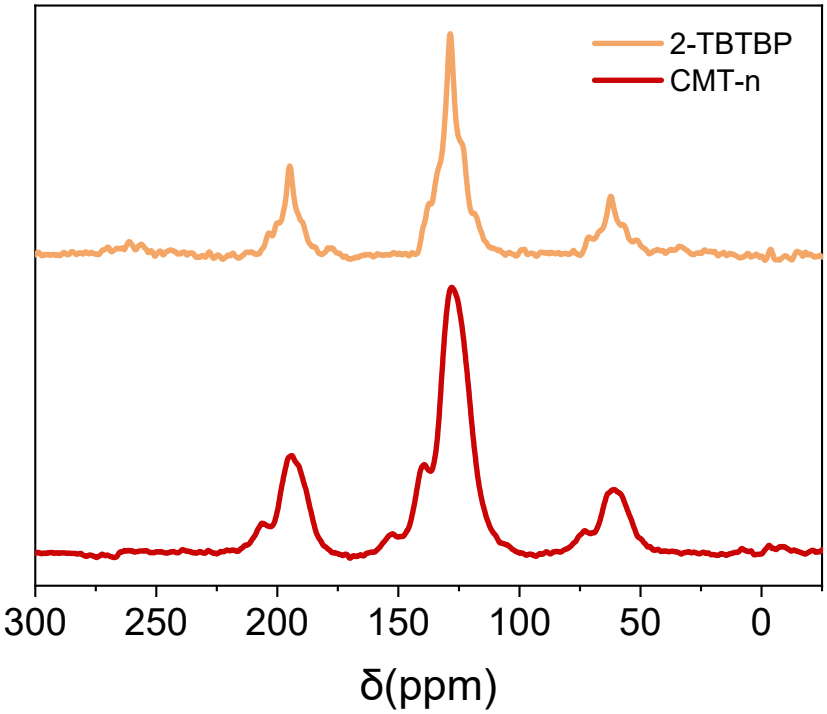

Figure S8. Solid state 13C NMR of 2-TBTBP and CMT-n. The ^{13}C solid-state NMR spectra of 2-TBTBP and CMT-n show similar peaks, which are consistent with previous reports of 2-TBTBP analogues. [1, 3]

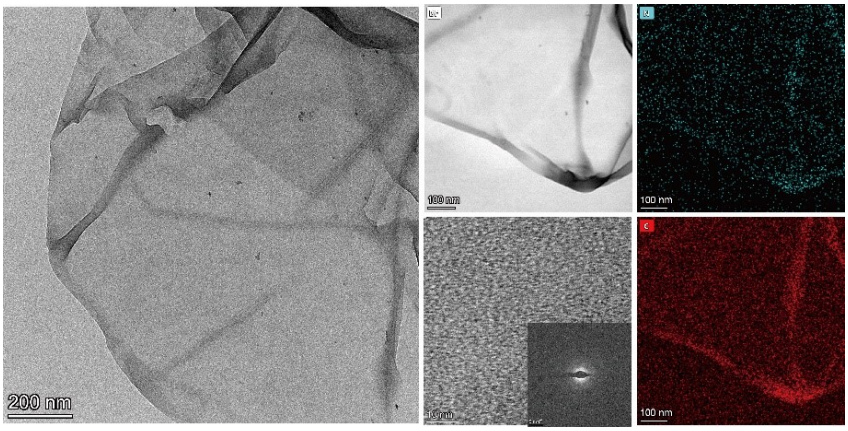

Figure S9. HR-TEM images of CMT-n and the corresponding EDS mappings for C and N atoms.

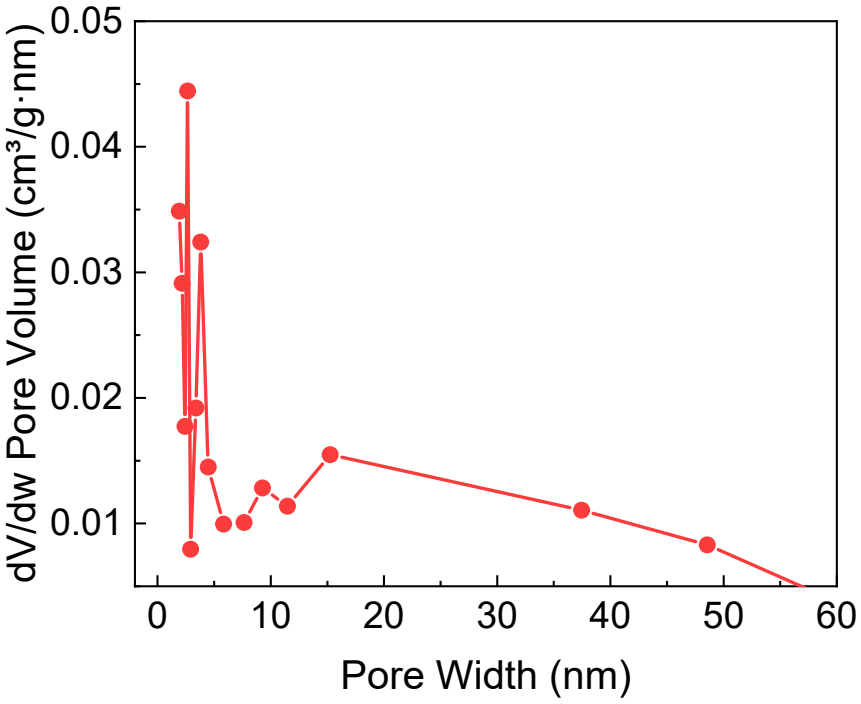

Figure S10. Pore size distribution of CMT-n calculated from the nitrogen adsorption data.

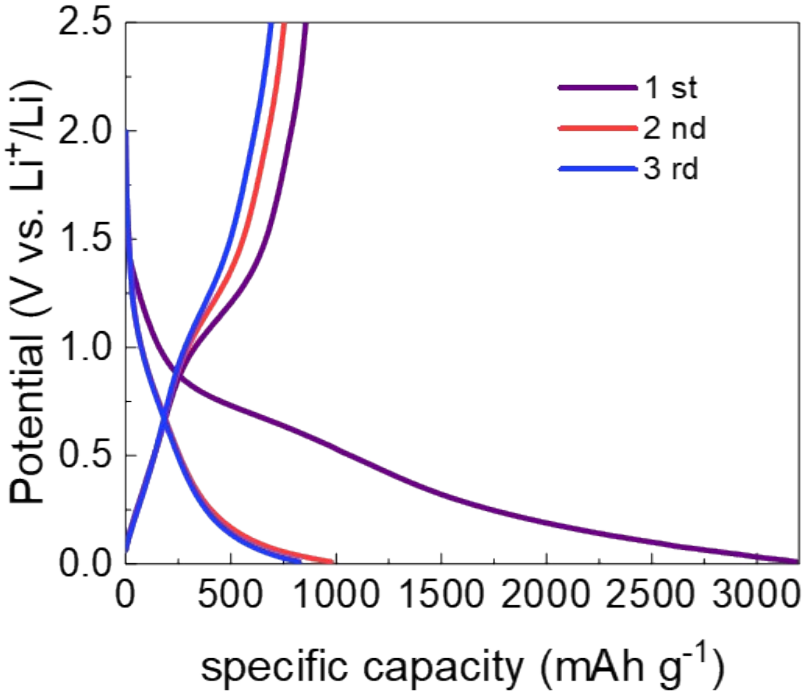

Figure S11. Galvanostatic charge-discharge profiles of CMT-n at the current density of 0.25 A g^{-1}

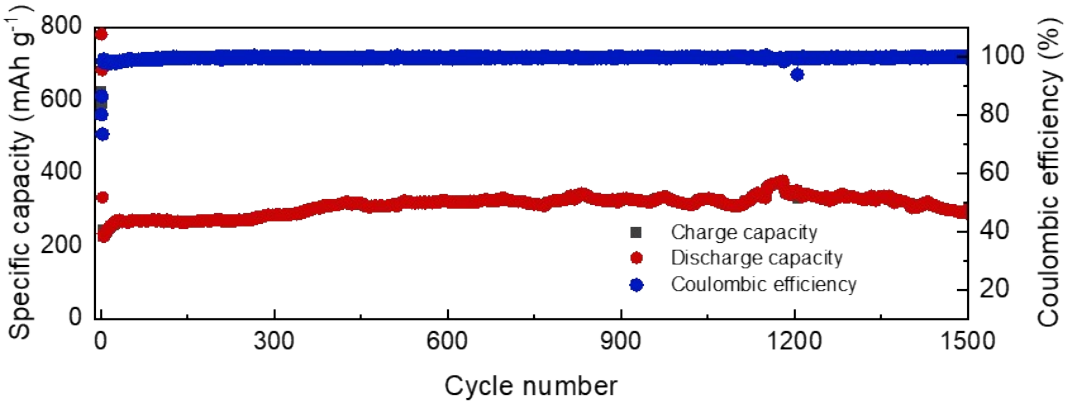

Figure S12. Long cycling performance of CMT-n at a current density of 3.0A g^{-1}.

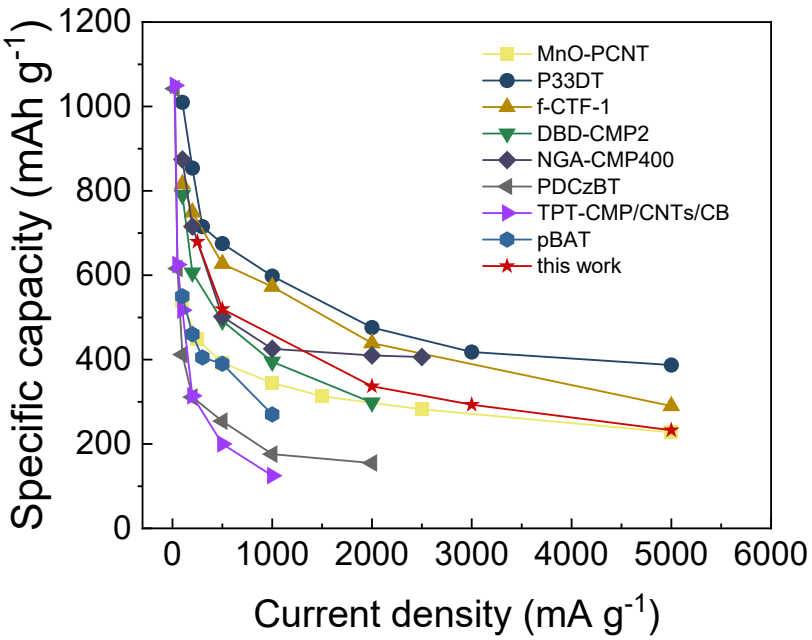

Figure S13. Comparative electrochemical performance of CMT-n and other CMP-based anodes.[4-11]

	CMT-n	
	E[a]	T[b]
C (wt%)	85.13	89.38
H (wt%)	2.9	3.18
N (wt%)	8.15	7.44
Br (wt%)	2.21	0
total	98.39[c]	100

Table S1. Residual amount of bromine in CMT-n measured by ICP-MS. [a] Experimental results. [b] Theoretical value. [c] The difference between experimental results and the theoretical value should be caused by trapped small molecules in the pores (oxygen, water and etc).

References

1. W. Liu, S.-D. Jiang, Y. Yan, W. Wang, J. Li, K. Leng, S. Japip, J. Liu, H. Xu, Y. Liu, I.-H. Park, Y. Bao, W. Yu, M. D. Guiver, S. Zhang and K. P. Loh, *Nature Communications*, 2020, **11**, 1633.
2. W. Liu, M. Ulaganathan, I. Abdelwahab, X. Luo, Z. Chen, S. J. Rong Tan, X. Wang, Y. Liu, D. Geng, Y. Bao, J. Chen and K. P. Loh, *ACS Nano*, 2018, **12**, 852-860.
3. W. Liu, X. Luo, Y. Bao, Y. P. Liu, G.-H. Ning, I. Abdelwahab, L. Li, C. T. Nai, Z. G. Hu, D. Zhao, B. Liu, S. Y. Quek and K. P. Loh, *Nature Chemistry*, 2017, **9**, 563-570.
4. S. Zhang, W. Huang, P. Hu, C. Huang, C. Shang, C. Zhang, R. Yang and G. Cui, *Journal of Materials Chemistry A*, 2015, **3**, 1896-1901.
5. Q. Zhang, Q. Dai, M. Li, X. Wang and A. Li, *Journal of Materials Chemistry A*, 2016, **4**, 19132-19139.
6. C. Zhang, Y. He, P. Mu, X. Wang, Q. He, Y. Chen, J. Zeng, F. Wang, Y. Xu and J.-X. Jiang, *Advanced Functional Materials*, 2018, **28**, 1705432.
7. L. Meng, S. Ren, C. Ma, Y. Yu, Y. Lou, D. Zhang and Z. Shi, *Chemical Communications*, 2019, **55**, 9491-9494.
8. Y. Zhu, X. Chen, Y. Cao, W. Peng, Y. Li, G. Zhang, F. Zhang and X. Fan, *Chemical Communications*, 2019, **55**, 1434-1437.
9. N. Xu, S. Mei, Z. Chen, Y. Dong, W. Li and C. Zhang, *Chemical Engineering Journal*, 2020, **395**, 124975.
10. T. Yang, C. Zhang, W. Ma, X. Gao, C. Yan, F. Wang and J.-X. Jiang, *Solid State Ionics*, 2020, **347**, 115247.
11. S. Mushtaq, F. Meng, Z. Zhang, Z. Wang, B. Jiang, B. Xue and F. Zhang, *Journal of Materials Chemistry A*, 2023, **11**, 17217-17225.